Inorganic Chemistry

Article

pubs.acs.org/IC

Dilution-Triggered SMM Behavior under Zero Field in a Luminescent Zn_2Dy_2 Tetranuclear Complex Incorporating Carbonato-Bridging Ligands Derived from Atmospheric CO_2 Fixation

Silvia Titos-Padilla,[†] José Ruiz,[†] Juan Manuel Herrera,[†] Euan K. Brechin,[‡] Wolfgang Wernsdorfer,[§] Francesc Lloret,[⊥] and Enrique Colacio*,[†]

[†]Departamento de Química Inorgánica, Facultad de Ciencias, Universidad de Granada, Avenida Fuentenueva s/n, 18071 Granada, Spain

[‡]EaStCHEM School of Chemistry, The University of Edinburgh, West Mains Road, Edinburgh EH9 3JJ, U.K.

[§]Institut Néel-CNRS, Grenoble 38042, France

[⊥]Instituto de Ciencia Molecular (ICMOL), Universitat de València, 46980 Paterna, València, Spain

Supporting Information

ABSTRACT: The synthesis, structure, magnetic, and luminescence properties of the Zn_2Dy_2 tetranuclear complex of formula $\{(\mu_3\text{-}CO_3)_2[Zn(\mu\text{-L})Dy(NO_3)]_2\}\cdot 4CH_3OH$ (**1**), where H_2L is the compartmental ligand *N*,*N*′,*N*″-trimethyl-*N*,*N*″-bis(2-hydroxy-3-methoxy-5-methylbenzyl)diethylenetriamine, are reported. The carbonate anions that bridge two Zn(μ-L)Dy units come from the atmospheric CO_2 fixation in a basic medium. Fast quantum tunneling relaxation of the magnetization (QTM) is very effective in this compound, so that single-molecule magnet (SMM) behavior is only observed in the presence of an applied dc field of 1000 Oe, which is able to partly suppress the QTM relaxation process. At variance, a 1:10 Dy:Y magnetic diluted sample, namely, **1**′, exhibits SMM behavior at zero applied direct-current (dc) field with about 3 times higher thermal energy barrier than that in **1** (U_{eff} = 68 K), thus demonstrating the important role of intermolecular dipolar interactions in favoring the fast QTM relaxation process. When a dc field of 1000 Oe is applied to **1**′, the QTM is almost fully suppressed, the reversal of the magnetization slightly slows, and U_{eff} increases to 78 K. The dilution results combined with micro-SQUID magnetization measurements clearly indicate that the SMM behavior comes from single-ion relaxation of the Dy^{3+} ions. Analysis of the relaxation data points out that a Raman relaxation process could significantly affect the Orbach relaxation process, reducing the thermal energy barrier U_{eff} for slow relaxation of the magnetization.

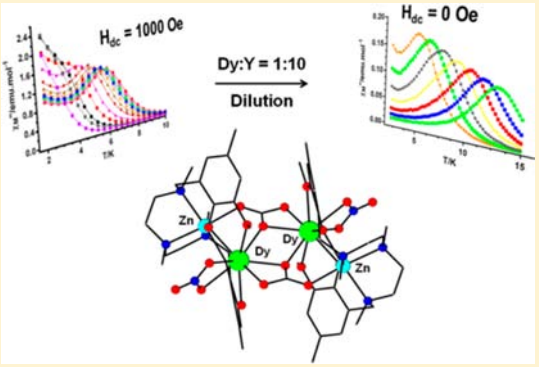

INTRODUCTION

The discovery of molecular complexes that can function as single-domain nanoparticles, by exhibiting slow relaxation of the magnetization and magnetic hysteresis below the so-called blocking temperature (T_B), stimulated research activity in the field of the molecular magnetism based on coordination compounds. These chemically and physically fascinating nanomagnets, called single-molecule magnets (SMMs),[1,2] straddle the quantum/classical interface showing quantum effects, such as quantum tunneling of the magnetization (QTM) and quantum phase interference, and have been suggested for applications in molecular spintronics, ultrahigh-density magnetic information storage,[3] and quantum computing at the molecular level.[4] The driving force behind the enormous increase of activity in the field of SMMs is the prospect of integrating them in nanosized devices.[5] The origin of the SMM behavior is the existence of an energy barrier (U) that prevents reversal of the molecular magnetization when the field is removed, leading to bistability.[1] Heightened U values can be obtained by increasing the spin multiplicity of the ground state (S_T) or the easy-axis (or Ising-type) magnetic anisotropy of the entire molecule ($D < 0$). Nevertheless, it is very complicated to simultaneously increase both parameters in transition-metal clusters because they are interrelated, so that when S_T is very large (observed for high-nuclearity clusters), D tends to be low. Consequently, the currently observed energy barriers are low, and therefore SMMs act as magnets only at very low temperature. Recently, researchers focused their attention on lanthanide (Ln) ions (and actinide) because they have large intrinsic magnetic anisotropy and large magnetic moments in the ground state and therefore could lead to metal complexes with higher energy barriers and improved SMM properties.[6,7] Thus, mixed 3d/4f metal aggregates[2,8] and low-

Received: May 31, 2013
Published: August 8, 2013

   dx.doi.org/10.1021/ic401378k | *Inorg. Chem.* 2013, 52, 9620−9626

nuclearity 4f metal complexes[6,9] have been reported to exhibit slow relaxation of the magnetization with U and T_B values as high as 790 cm^{-1} and 14 K, respectively.[10,11] It should be noted that fast QTM relaxation processes mediated by dipolar interactions, transverse anisotropy, or hyperfine interactions can reduce the energy barrier to an effective value (U_{eff}), thus attenuating the SMM properties of the lanthanide-containing species.[1,6] However, in some cases, the exchange coupling between Ln ions, the dilution of the complex within a diamagnetic matrix to eliminate dipolar interactions,[12] and the application of a small static magnetic field,[13] to remove the mixing of the ground $\pm M_s$ levels, can partly or fully suppress the QTM relaxation processes, enabling observation of the slow relaxation process through the real thermally activated energy barrier (U).

We,[14] and others,[15] have experimentally shown that the very weak J_{M-Ln} observed for 3d/4f dinuclear complexes (M^{II} = Cu, Ni, and Co) leads to small separations of the low-lying split sublevels and consequently to a smaller energy barrier for magnetization reversal. In view of this, a good strategy to enhance the SMM properties of the 3d/4f aggregates would be that of eliminating the weak M^{2+}–Ln^{3+} interactions that split the ground sublevels of the Ln^{III} ion by replacing the paramagnetic M^{2+} ions by a diamagnetic ion.[15,16] According to this strategy, we are now pursuing the synthesis of 3d/4f systems in which the paramagnetic M^{2+} ions have been changed by diamagnetic Zn^{2+}.

Herein, we report the synthesis, X-ray structure, and detailed dc/ac magnetic susceptibility studies, including dilution and magnetic field dependence, of a $Zn^{II}_2Dy^{III}_2$ tetranuclear complex of $\{(\mu_3\text{-}CO_3)_2[Zn(\mu\text{-}L)Dy(NO_3)]_2\}\cdot 4CH_3OH$ (**1**), where H_2L is the compartmental ligand *N*,*N*′,*N*″-trimethyl-*N*,*N*″-bis(2-hydroxy-3-methoxy-5-methylbenzyl)-diethylenetriamine (see Figure 1). Compound **1** represents a rare example of a lanthanide-containing complex that undergoes a transformation from paramagnetic to high-energy-barrier SMM under zero field triggered only by diamagnetic dilution.

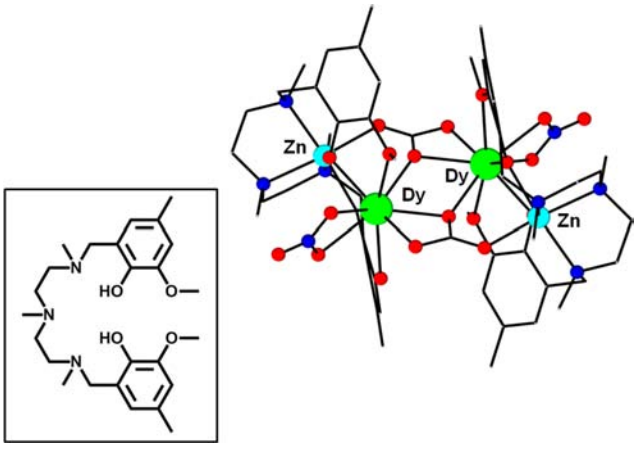

Figure 1. Structure of the ligand H_2L (inset) and a perspective view of the structure of **1**. Color code: N, blue; O, red; Zn, light blue; Dy, green; C, gray. H atoms have been omitted for clarity.

EXPERIMENTAL SECTION

Synthetic Procedures. The ligand was prepared as previously reported.[14a]

*$\{(\mu_3\text{-}CO_3)_2[Zn(\mu\text{-}L)Dy(NO_3)]_2\}\cdot 4CH_3OH$ (**1**).* To a solution of H_2L (56 mg, 0.125 mmol) in 5 mL of MeOH were subsequently added with continuous stirring 37.2 mg (0.125 mmol) of $Zn(NO_3)_2\cdot 6H_2O$, 54.8 mg (0.125 mmol) of $Dy(NO_3)_3\cdot 5H_2O$, and 12.6 mg of triethylamine (0.125 mmol). The resulting colorless solution was filtered and allowed to stand at room temperature. After 2 days, well-formed prismatic crystals of compound **1** were obtained with a yield of 45% based on Zn. Anal. Calcd for $C_{56}H_{90}N_8O_{24}Zn_2Dy_2$: C, 39.22; H, 5.29; N, 6.54. Found: C, 39.17; H, 5.56; N, 6.74. IR (KBr): 3430 (w), 2919 (w), 2863 (w), 1538 (s), 1491 (s), 1460 (m), 1384 (s), 1352 (m), 1321 (m), 1255 (m), 1070 (w), 848 (w), 812 (w), 797 (w) cm^{-1}.

*$\{(\mu_3\text{-}CO_3)_2[Zn(\mu\text{-}L)Dy_{0.126}Y_{0.874}(NO_3)]_2\}\cdot 4CH_3OH$ (**1′**).* This diluted complex was prepared by following the same method as that for **1** but using 0.0125 mmol of $Dy(NO_3)_3\cdot 5H_2O$ and 0.1125 mmol of $Y(NO_3)_3\cdot 6H_2O$ instead of 0.125 mmol of $Dy(NO_3)_3\cdot 5H_2O$. The colorless crystals of **1′** were obtained with a yield of 30% based on Zn. Anal. Calcd for $C_{56}H_{90}N_8O_{24}Zn_2Y_{1.75}Dy_{0.25}$: C, 42.40; H, 5.72; N, 7.06. Found: C, 42.41; H, 5.61; N, 7.44. The IR spectrum is virtually identical with that of **1**.

Physical Measurements. Elemental analyses were carried out at the "Centro de Instrumentación Científica" (University of Granada) on a Fisons-Carlo-Erba analyzer model EA 1108. IR spectra on powdered samples were recorded with a Thermo Nicolet IR200FTIR using KBr pellets.

Single-Crystal Structure Determination. Suitable crystals of **1** and **1′** were mounted on a glass fiber and used for data collection on a Bruker AXS APEX CCD area detector equipped with graphite-monochromated Mo Kα radiation (λ = 0.71073 Å) by applying the ω-scan method. Lorentz polarization and empirical absorption corrections were applied. The structure was solved by direct methods using the programs *SIR-97*[17] and *SHELXS97*[18] and refined with full-matrix least-squares calculations on F^2 using *SHELXS97*.[18] These programs were used with the package *WINGX*.[19] The heavy atoms were refined anisotropically. All H atoms were included at the calculated distances with fixed displacement parameters from their host atoms. The crystallographic data of **1′** refer to one crystal that contains Dy and Y ions in a ratio of 0.095:0.905, which are statistically distributed, so that the probabilities of observing ZnDyDyZn, ZnDyYZn, and ZnYYZn species are 0.009, 0.172, and 0.82, respectively. We have measured three crystals of the diluted complex **1′**, and in all cases, the refinements led to Dy/Y ratios of ∼1:10. Final $R(F)$, $R_w(F^2)$, and goodness-of-fit agreement factors, details on the data collection, and analysis can be found in Table S1 in the Supporting Information (SI). Selected bond lengths and angles are given in Table S2 in the SI.

Powder X-ray Diffraction Analysis. Crystals of **1** were gently ground in an agate mortar and then deposited with care in the hollow of an aluminum holder equipped with a zero back ground plate. Diffraction data (Cu Kα, λ = 1.5418 Å) were collected on a θ:θ Bruker AXS D8 vertical scan diffractometer equipped with primary and secondary Soller slits, a secondary beam-curved graphite monochromator, a Na(Tl)I scintillation detector, and pulse height amplifier discrimination. The generator was operated at 40 kV and 40 mA. A scan was performed with $5 < 2\theta < 30°$ with t = 5 s and $\Delta 2\theta = 0.02°$. LeBail refinement was obtained with the aid of *TOPAS-R*[20] [triclinic, $P\bar{1}$ as the space group, a = 11.66 Å, b = 12.68 Å, c = 14.16 Å, α = 111.19°, β = 104.19°, and γ = 99.19°], verifying the purity of the sample.

Magnetic Properties. The variable-temperature (2–300 K) magnetic susceptibility measurements on polycrystalline samples of **1** and **1′** under an applied field of 1000 Oe were carried out with a Quantum Design SQUID MPMS XL-5 device. Alternating-current (ac) susceptibility measurements under different applied static fields were performed using an oscillating ac field of 3.5 Oe and ac frequencies ranging from 1 to 1500 Hz. ac magnetic susceptibility measurements in the range 1–10000 Hz were carried out with a Quantum Design Physical Property Measurement System using an oscillating ac field of 5 Oe. The experimental susceptibilities were corrected for the sample holder and diamagnetism of the constituent atoms using Pascal's tables. A pellet of the sample cut into very small

dx.doi.org/10.1021/ic401378k | Inorg. Chem. 2013, 52, 9620–9626

pieces was placed in the sample holder to prevent any torquing of the microcrystals.

RESULTS AND DISCUSSION

Complex **1** was prepared from the reaction of H_2L with $Zn(NO_3)_2{\cdot}6H_2O$ and subsequently with $Dy(NO_3)_3{\cdot}5H_2O$ and triethylamine in MeOH using a 1:1:1:1 molar ratio. Colorless prismatic-shaped crystals of **1** suitable for X-ray analysis were slowly grown from the solution.

The centrosymmetric tetranuclear structure of **1** (see Figure 1 and Tables S1 and S2 in the SI for crystallographic details) consists of two $[Zn(\mu\text{-L})Dy(NO_3)]$ dinuclear units connected by two tetradentate carbonate bridging ligands acting with a μ_3-κ^2-O,O′:κ-O:κ-O″ coordination mode. The chelating part of the carbonato ligand is coordinated to the Dy^{3+} ion of a dinuclear entity, whereas the remaining O atom is coordinated to the Zn^{2+} ion of the centrosymmetrically related dinuclear unit. Notice that one of the O atoms of the chelating part of each carbonato ligand bridges the two Dy^{3+} ions in a nonsymmetric form, giving rise to a rhomboidal $Dy(O)_2Dy$ bridging unit with a Dy−O−Dy bridging angle of 115.72° and two different Dy−O distances of 2.360 and 2.419 Å. The carbonato ligand is presumably generated from the fixation of atmospheric CO_2 in a basic medium through the nucleophilic attack of hydroxo species bound to the Ln ions (derived from deprotonation of the coordinated water molecules) to the electrophilic C atom of CO_2. Similar processes occurring in a basic medium have been observed for other carbonate-bridged Dy^{3+} polynuclear complexes.[21,22] The presence of CO_3^{2-} instead of NO_3^- in **1** was proven, apart from charge balance, by IR spectroscopy, because this compound exhibits, compared to the dinuclear one $[Zn(H_2O)(\mu\text{-L})Dy(NO_3)_3]{\cdot}H_2O$ (prepared in the same conditions as those for **1** but without using triethylamine), a new band at 1538 cm^{-1} assignable to a C−O stretching vibration of the CO_3^{2-} anion (see Figure S1 in the SI). The same IR band has been observed for other carbonato-bridged Zn−Ln complexes.[23] Powder X-ray diffraction measurements were carried out on a polycrystalline sample obtained by grinding a crop of crystals of **1**. The experimental X-ray diffractogram matches very well with the theoretical one obtained from the X-ray single-crystal structure data (see Figure S2 in the SI), thus proving the purity of **1**.

Within each of the $[Zn(\mu\text{-L})Dy(NO_3)]$ dinuclear units, Zn^{2+} and Dy^{3+} ions are bridged by two phenoxo groups of the L^{2-} ligand, which wrap around the Zn^{2+} ion in such a way that the three N atoms from the amine groups, and consequently the three O atoms belonging to the carbonato and phenoxo bridging groups, occupy *fac* positions on the slightly trigonally distorted ZnN_3O_3 coordination polyhedron. The Dy^{3+} ion exhibits a rather nonsymmetrical DyO_9 coordination, which is made by two phenoxo bridging O atoms, two methoxy O atoms, three O atoms from the carbonato bridging groups, and two O atoms belonging to a bidentate nitrate anion. The latter and the chelating part of the carbonato ligand occupy cis positions on the Dy^{3+} coordination sphere. The Dy−O distances are in the range 2.280−2.559 Å. In the bridging fragment, the $Dy(O)_2Dy$ and carbonato planes are not coplanar, having a dihedral angle of 28.6°. The tetranuclear molecules $\{(\mu_3\text{-}CO_3)_2[Zn(\mu\text{-LDy}(NO_3)]_2\}$ are well separated in the structure by methanol molecules, with the shortest Dy···Dy distance being 12.33 Å. One of the methanol molecules forms bifurcated hydrogen bonds with one of the O atoms of the chelating part of the carbonato ligand and the O atom of the other methanol molecule, with donor−acceptor distances of 2.672 and 2.601 Å, respectively. It should be noted that very recently Tang et al. reported a similar Zn_2Dy_2 tetranuclear complex.[22] The most significant differences between this complex and **1** are as follows: (i) In the former complex, the carbonate bridging fragment is planar, whereas in **1**, it is not. (ii) The Dy−O bond distances and Dy−O−Dy angles in the former complex are respectively shorter and larger than those found in **1**. (iii) Tang's complex has five almost coplanar O atoms around the Dy^{3+} ions, whereas in **1**, these five O atoms significantly deviate from the mean plane. (iv) Complex **1** has a bidentate nitrate ligand coordinated to each Dy^{3+} ion, whereas Tang's complex contains bidentate acetate ligands. The two former points favor a stronger Dy···Dy magnetic exchange interaction through the carbonate bridging groups in Tang's complex than in **1**, whereas point iii favors a larger axial anisotropy in the former.

The direct-current (dc) magnetic susceptibility of **1** has been measured in the 2−300 K temperature range under an applied magnetic field of 0.1 T (Figure S3 in the SI). The $\chi_M T$ value of 30.15 cm^3 K mol^{-1} at 300 K is compatible with the calculated value of 28.34 cm^3 K mol^{-1} for two noncoupled Dy^{3+} ions ($4f^9$, $J = {}^{15}/_2$, $S = {}^5/_2$, $L = 5$, $g = {}^4/_3$, ${}^6H_{15/2}$) in the free-ion approximation. Upon cooling, the $\chi_M T$ product steadily decreases to reach a value of 22.13 cm^3 K mol^{-1} at 2 K. This behavior is due to depopulation of the Stark sublevels of the Dy ion, which arise from splitting of the ${}^6H_{15/2}$ ground-state term by the ligand field rather than from very weak intramolecular interactions between the Dy^{III} ions, because the isostructural Zn_2Gd_2 complex exhibits weak intramolecular ferromagnetic magnetic exchange interaction between the Gd^{3+} ions.[24] For the similar Zn_2Dy_2 complex reported by Tang et al., an increase in $\chi_M T$ is observed below 50 K, thus indicating that the Dy···Dy ferromagnetic interaction in this complex is stronger than that found for **1**. The *M* versus *H* plot at 2 K (Figure S3 in the SI, right inset) shows a relatively rapid increase in the magnetization at low field and then a very slow linear increase to reach a value of 11.54 $N\mu_B$ at the maximum applied field of 5 T. This behavior suggests the presence of a significant magnetic anisotropy and/or more likely the presence of low-lying excited states that are partially (thermally and field-induced) populated. These low-lying excited states are in agreement with weak magnetic interactions expected for 4f−4f systems. The magnetization value per Dy^{3+} ion at 5 T is considerably smaller than the expected saturation value for one free Dy^{3+} ion of 10 $N\mu_B$ ($M_s/N\mu_B = g_J J = 10\ N\mu_B$) and is similar to those estimated and observed for other Dy^{III} mononuclear complexes with approximate axial symmetry. This behavior is likely due to crystal-field effects, leading to significant magnetic anisotropy, which eliminates the 16-fold degeneracy of the ${}^6H_{15/2}$ ground state. Notice that the field dependence of magnetization shows no significant hysteresis above 2 K with the sweep rates used in the SQUID magnetometer.

Dynamic ac magnetic susceptibility measurements as a function of the temperature and frequency for **1** are given in Figures 2 and S4 in the SI, respectively.

In spite of the expected large anisotropy of the Dy^{3+} ion, this complex did not show any out-of-phase (χ''_M) signal under zero external field, which can be attributed to the presence of fast relaxation of the magnetization via a QTM mechanism through the thermal energy barrier between degenerate energy levels. As for noninteger spin systems, like Dy^{3+}, transverse anisotropy would not facilitate QTM; this would be mainly mediated by

dx.doi.org/10.1021/ic401378k | Inorg. Chem. 2013, 52, 9620−9626

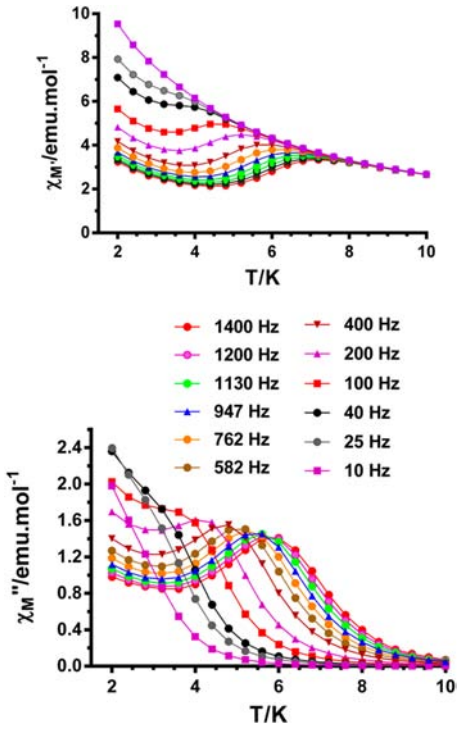

Figure 2. Temperature dependence of the in-phase χ_M' (top) and out-of-pahse χ_M' (bottom) ac signals under an applied dc field of 1000 Oe for **1**. Solid lines are guides for the eye.

dipole−dipole and/or hyperfine interactions. The similar Zn_2Dy_2 tetranuclear complex reported by Tang et al. shows out-of-phase signals with maxima below 8 K at zero field and therefore SMM behavior with U_{eff} = 34 K.[22] The suspected larger anisotropy of the Dy^{3+} ion as well as the stronger Dy···Dy magnetic exchange interaction for this compound compared to **1** may be the reason why slow relaxation of the magnetization is observed at zero field. In fact, exchange coupling has been found to reduce quantum tunneling of the magnetization at zero applied field.[11]

However, when a small static field of 1000 Oe is applied to fully or partly suppress the QTM relaxation (this field was chosen because under its application the relaxation process was shown to be the slowest), compound **1** shows slow relaxation of the magnetization, as is demonstrated by the appearance below 10 K of out-of-phase peaks in the 3.5−6 K (100−1400 Hz) range. Both χ'_M and χ''_M components (Figure 2) do not go to zero below the maxima at low temperature, which can be taken as a clear indication that the QTM has not been efficiently suppressed.

The Cole−Cole diagram for **1** in the temperature range 4−6 K (Figure S5 in the SI) exhibits semicircular shapes and can be fitted using the generalized Debye model, affording α values (this parameter determines the width of the distribution of relaxation times, so that α = 1 corresponds to an infinitely wide distribution of relaxation times, whereas α = 0 represents a relaxation with a single time constant) in the range 0.23−0.06, which suggest the existence of more than one relaxation process operating at low temperatures. The larger α values are associated with the tunneling regime because the QTM relaxation is more susceptible to local strain and/or disorder than the Orbach thermally activated relaxation. The set χ_0 (isothermal susceptibility), χ_S (adiabatic susceptibility), and α obtained in the above fits were further used to fit the frequency dependence of χ_M' at each temperature to the generalized Debye model, which permits the relaxation time τ to be extracted. The results were then used in the construction of the Arrhenius plot shown in Figure 3 and in the inset of Figure S2

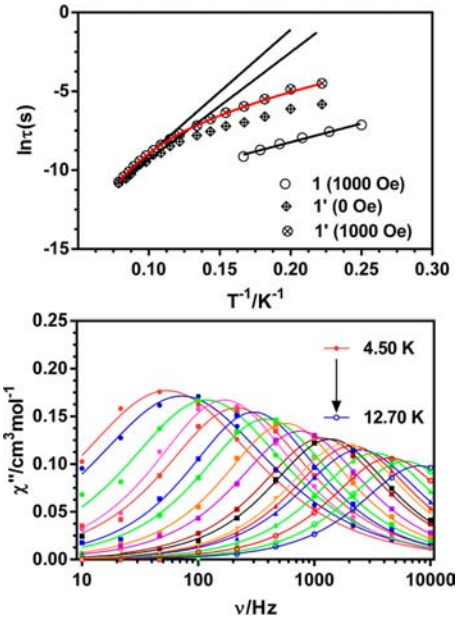

Figure 3. Top: Arrhenius plots of relaxation times of **1** under 1 kOe and **1′** under 0 and 1 kOe. Black solid lines represent the best fit of the experimental data to the Arrhenius equation. The red line represents the best fit to a Orbach plus Raman relaxation process. Bottom: Temperature dependence of the molar out-of-phase ac susceptibility (χ_M') for **1′** under 0 Oe dc applied field. Solid lines represent the best fit of the experimental data to the Debye model.

in the SI. The fit of the data afforded an effective energy barrier for reversal of magnetization of 24(1) K with $\tau_0 = 2.3 \times 10^{-6}$ s. The Arrhenius plot, constructed from the temperatures and frequencies of the maxima observed for the χ''_M signals in Figure 2, leads virtually to the same result, as expected. In order to know how the intermolecular magnetic dipolar interactions influence the relaxation in compound **1**, we performed ac susceptibility measurements on a magnetic diluted sample **1′** (Figures 3 and 4), which was prepared through crystallization with the diamagnetic and isostructural yttrium complex (see the SI for the crystallographic data) using a Dy/Y molar ratio of 1:10 (the amount of Dy present in the dilute sample was determined to be the 12.6% from the low-temperature portions of the dc susceptibility for the dilute and neat compounds and is not far from that extracted from X-ray results of 9.5%). Interestingly, compound **1′** shows slow relaxation of the magnetization even under zero field (Figures 3 and 4) with out-of-phase peaks in the 5−13 K (100−10000 Hz) range. The relaxation times were extracted from the fitting of the frequency-dependent ac data between 4.5 and 12.7 K, and they follow Arrhenius behavior in the 12.7−8.7 K range with U_{eff} = 68(4) K and $\tau_0 = 9.8 \times 10^{-8}$ s. The Cole−Cole plot (Figure S6 in the SI) shows in the latter temperature region semicircular shapes with α values in the range 0.04−0.07, thus indicating the presence of a very narrow distribution of slow relaxation in that region. The dramatic increase of the thermal energy barrier in **1′** with regard to **1**, with a concurrent decrease in τ_0, indicates that suppression of intermolecular interactions leads to slower relaxation of the magnetization and SMM

dx.doi.org/10.1021/ic401378k | Inorg. Chem. 2013, 52, 9620−9626

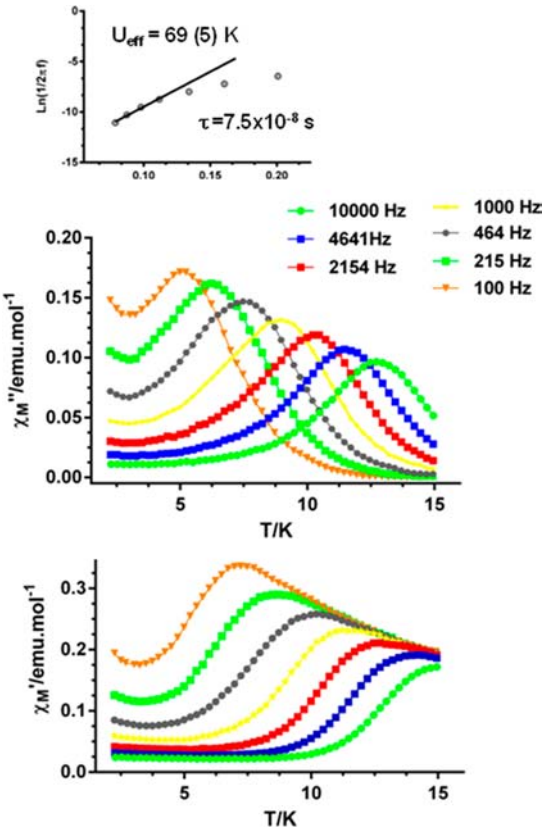

Figure 4. Temperature dependence of the in-phase χ_M' (bottom) and out-of-phase χ_M'' (medium) ac signals at zero applied dc field for **1′** at different frequencies. The Arrhenius plot for **1′** was constructed from the temperatures of the maxima and the corresponding frequencies.

behavior at zero field. The significant U_{eff} thermal energy barrier observed for **1′** is found in the high end of the U_{eff} values observed for mono- and polynuclear Dy-SMMs.[9]

Even after dilution, a nonnegligible fast tunneling relaxation is observed at low temperatures and frequencies at zero field, as indicated by the divergence in χ''_M below the maxima in the χ''_M versus T plot at different frequencies (Figure 4). After application of a small static field of 1000 Oe, which induces the slowest relaxation process, the QTM is almost suppressed (Figures S7 and S8 in the SI) and the fit of the relaxation times versus $1/T$ data in the 12.7−9.2 K temperature range to the Arrhenius law leads (see Figure 3, top), as expected, to a slight increase of the thermal energy barrier and a decrease of τ_0 [U_{eff} = 78(2) and $\tau_0 = 4.7 \times 10^{-8}$ s]. In the above temperature region, the α values extracted from the Cole−Cole plot (Figure S9 in the SI) are in the 0.03−0.08 range, which also supports the presence of a very narrow distribution of slow relaxation in the high-temperature region. Nevertheless, the fact that, under an applied magnetic field of 1 kOe, when the QTM is almost suppressed, the experimental relaxation times deviate from the Orbach linear law in the 4.5−12.7 K temperature region, could indicate the presence of multiple relaxation processes. In view of this, we have fitted the experimental data to the following equation, which considers that the spin−lattice relaxation takes place through Raman and Orbach processes:[25]

$$\tau^{-1} = BT^n + \tau_0^{-1} \exp(-U_{eff}/kT)$$

The first and second terms correspond to the Raman and Orbach processes, respectively. In general, n = 9 for Kramers ions,[25] but depending on the structure of the levels, n values between 1 and 6 can be considered as reasonable.[26] The best fit of the experimental data in the above temperature range affords n = 5.2(3), B = 0.04(2), $\tau_0 = 2.5 \times 10^{-8}$, and U_{eff} = 121(4) K (Figure 3, top, red line). These results seem to indicate that the Raman relaxation process significantly affects the Orbach relaxation process, reducing the thermal energy barrier U_{eff} for slow relaxation of the magnetization.

We have performed magnetization hysteresis loop measurements in the 0.03−4 K temperature range using a μ-SQUID instrument[27] with the aim of studying the magnetization dynamics and to confirm the SMM properties of **1** and **1′**. Magnetization versus applied dc field hysteresis loops at different temperatures and sweeping rates are given in Figure 5. Hysteresis loops were measured on single crystals, which

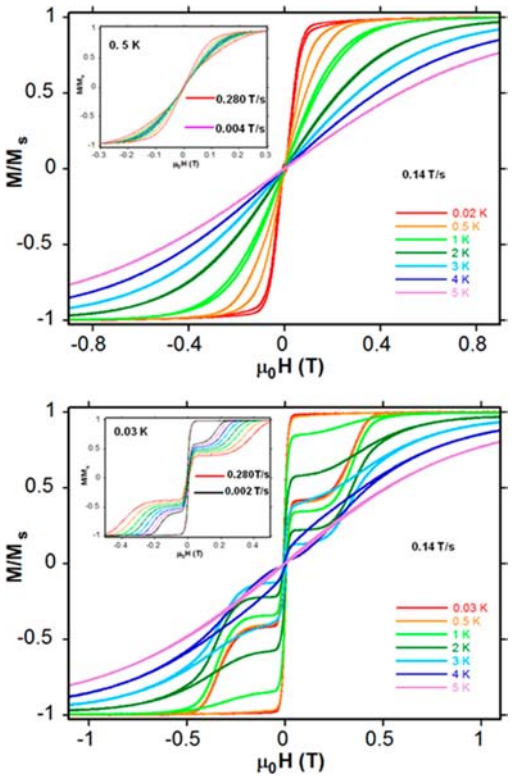

Figure 5. Top: Normalized magnetizations (M/M_s) versus applied dc field sweeps at the indicated sweep rate and temperatures for **1**. Inset: Using sweep rates between 0.004 and 0.280 T/s at 0.03 K. Bottom: Same plots for **1′**.

were aligned with the easy axis of magnetization using the transverse field method.[28] For **1**, a large step is observed at zero field without hysteresis (Figure 5a), which is consistent with the QTM generally found for 4f-containing complexes and with the tail that exhibits this compound at low temperature in the χ_M'' versus T plot. When the field is increased, below 1 K, hysteresis loops are observed with a small opening, with their coercitivities being temperature- and field-sweep-rate-dependent. The maximum opening occurs below 1500 Oe, which agrees well with the ac optimum field of 1000 Oe. As expected for SMM, the coercitivity increases with decreasing temperature and increasing field sweep rates. Surprisingly, below 0.5 K, the coercive field decreases with decreasing temperature. This behavior has been observed for other Dy-containing SMMs and

dx.doi.org/10.1021/ic401378k | Inorg. Chem. 2013, 52, 9620−9626

ascribed to a reduction of the tunneling due to thermal activations around the tunnel splitting.[29]

For the 1:10 diluted complex **1′**, two-step butterfly-shaped hysteresis loops were observed below 4 K (Figure 5b), whose coercitivity, as expected, increases with decreasing temperature and increasing field sweep rates. The fact that there exists significant coercive field at zero field for **1′** demonstrates that (i) the magnetic site doping can significantly suppress the QTM and (ii) the hysteresis is essentially a single-ion feature rather than a result of long-range ordering or magnetic interactions. In fact, for a 1:10 Dy/Y diluted system, the probability of observing the dinuclear species ZnDyYZn is 0.18, whereas that of the ZnDyDyZn species is only 0.01.

Finally, it should be noted that, upon excitation at the ligand (270 nm), the solid-state photoluminescence spectrum of **1** (Figure 6) exhibits two emission bands at 484 and 575 nm,

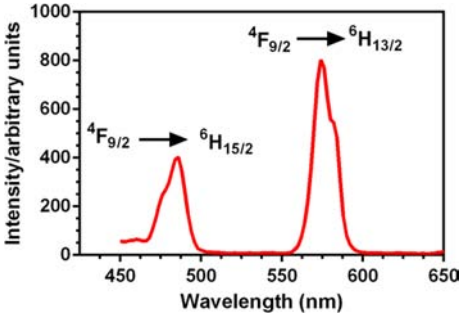

Figure 6. Solid-state photoluminescence spectrum of **1**.

respectively, which correspond with the characteristic emission $^4F_{9/2} \rightarrow {}^6H_J$ ($J = {}^{15}/_2, {}^{13}/_2$) transitions of the Dy^{3+} ion. The yellow emission intensity of the $^4F_{9/2} \rightarrow {}^6H_{13/2}$ transition is much stronger than the blue one of $^4F_{9/2} \rightarrow {}^6H_{15/2}$, suggesting that the ligand is suitable for the sensitization of yellow luminescence of Dy^{3+}. The emission spectrum of **1** is identical but much more intense than that observed for the mononuclear complex $[Dy(H_2L)(NO_3)_3]$,[13] which could be due to deprotonation of the ligand and coordination of the Zn^{2+} ion, altering the electronic energy levels of the ligand and improving energy transfer to the excited level of the Dy^{3+} ion.

CONCLUSION

We have been able to prepare a tetranuclear Zn_2Dy_2 complex, **1**, from reaction of the compartmental ligand H_2L (*N*,*N*′,*N*″-trimethyl-*N*,*N*″-bis(2-hydroxy-3-methoxy-5-methylbenzyl)-diethylenetriamine) with Zn^{2+} and further with Dy^{3+} in a 1:1 molar ratio and triethylamine. The Zn^{2+} ion occupies the internal N_2O_3 site, whereas the oxophilic Dy^{3+} ion shows preference for the O_4 external site, giving rise to the commonly found diphenoxo-bridged ZnDy dinuclear species. In a basic medium, carbonate ions are formed from atmospheric CO_2 and bridge two of these dinuclear units, affording the final Zn_2Dy_2 tetranuclear complex. This complex does not show slow relaxation of the magnetization at zero field due to fast QTM relaxation processes. However, in the presence of a small external dc field, the QTM is partly inhibited and the compound exhibits SMM behavior with an effective thermal barrier U_{eff} = 24 K. Interestingly, the diluted complex crystallized using a 1:10 Dy/Y ratio was shown to almost eliminate the QTM, indicating that it occurs by intermolecular dipolar interactions. In this case, SMM behavior is observed at zero field with almost a 3 times higher thermal energy barrier (U_{eff} = 68 K). This is one of the few examples of Dy^{3+} complexes where the SMM behavior is triggered by dilution. The magnetization study of the diluted complex at low temperatures clearly shows that slow relaxation of the magnetization is due to the single-ion relaxation of the Dy^{3+} ion. Even after dilution and in the presence of an applied magnetic field, when the QTM is suppressed (U_{eff} = 78 K), the experimental relaxation times deviate from the Orbach linear law, indicating the presence of multiple relaxation processes. It seems that the Raman relaxation process significantly affects the Orbach relaxation process, reducing the thermal energy barrier U_{eff} for slow relaxation of the magnetization. Finally, the luminescence spectrum of **1** suggests that the ligand is suitable for the sensitization of yellow luminescence of Dy^{3+}. Therefore, complex **1** can be considered as a bifunctional material, exhibiting both SMM behavior and luminescence properties.

We are now pursuing the preparation of new examples of Zn^{2+}−Ln^{3+} complexes with reduced intermolecular interactions that could eventually exhibit suppressed QTM, higher thermal energy barriers at zero field, and therefore improved SMM behavior. Work along this line is currently going on in our laboratories.

ASSOCIATED CONTENT

Supporting Information

Syntheses of the complexes, experimental details, X-ray crystallographic data for **1** and **1′**, including data collection, refinement, and selected bond lengths and angles, magnetic data, including dc and ac plots, Cole−Cole plots, and hysteresis plots, and CIF files. This material is available free of charge via the Internet at http://pubs.acs.org.

AUTHOR INFORMATION

Corresponding Author

*E-mail: ecolacio@ugr.es.

Notes

The authors declare no competing financial interest.

ACKNOWLEDGMENTS

Financial support from the Spanish Ministerio de Ciencia e Innovación (MICINN; Project CTQ-2011-24478), the Junta de Andalucía (FQM-195; Projects of Excellence P08-FQM-03705 and P11-FQM-7756), and the University of Granada (Project GREIB-PYR-2011-13 and Precompetitive Research Projects Programs ref.-07102011) is acknowledged. S.T.-P. thanks the Junta de Andalucía for a research grant. E.K.B. thanks the EPSRC and Leverhulme Trust for funding. F.L. thanks the MICINN (Project CTQ2010-15364), the University of Valencia (Project UV-INVAE11- 38904), and the Generalitat Valenciana (Projects PROMETEO/2009/108, GV/2012/051, and ISIC/2012/002) for financial support. W.W. acknowledges the ERC Advanced Grant MolNanoSpin No. 226558. The authors are grateful to A. Molina, CIC, University of Granada, and Dr. A. Rodríguez-Diéguez, Department of Inorganic Chemistry, University of Granada, for their help with magnetic measurements and powder X-ray measurements analysis, respectively.

DEDICATION

This paper is dedicated to Prof. Antonio Laguna, Department of Inorganic Chemistry, University of Zaragoza, Spain, on the occasion of his retirement.

REFERENCES

(1) Gatteschi, D.; Sessoli, R.; Villain, J. *Molecular Nanomagnets*; Oxford University Press: Oxford, U.K., 2006.

(2) (a) Aromí, G.; Brechin, E. K. *Struct. Bonding (Berlin)* **2006**, *122*, 1. (b) Bagai, R.; Christou, G. *Chem. Soc. Rev.* **2009**, *38*, 1011. (c) Molecular Magnets themed issue: Brechin, , E. K. *Dalton Trans.* **2010**,

(3) (a) Rocha, A. R.; García-Suárez, V. M.; Bailey, S. W.; Lambert, C. J.; Ferrerand, J.; Sanvito, S. *Nat. Mater.* **2005**, *4*, 335. (b) Bogani, L.; Wernsdorfer, W. *Nat. Mater.* **2008**, *7*, 179. (c) Affronte, M. *J. Mater. Chem.* **2009**, *19*, 1731.

(4) (a) Leuenberger, M. N.; Loss, D. *Nature* **2001**, *410*, 789. (b) Ardavan, A.; Rival, O.; Morton, J. J. L.; Blundell, S. J.; Tyryshkin, A. M.; Timco, G. A.; Winpenny, R. E. P. *Phys. Rev. Lett.* **2007**, *98*, 057201. (c) Stamp, P. C. E.; Gaita-Ariño, A. *J. Mater. Chem.* **2009**, *19*, 1718.

(5) (a) Candini, A.; Klyatskaya, S.; Ruben, M.; Wernsdorfer, W.; Affronte, M. *Nano Lett.* **2011**, *11*, 2634. (b) Vincent, R.; Klyatskaya, S.; Ruben, M.; Wernsdorfer, W.; Balestro, F. *Nature* **2012**, *488*, 357. (c) Ganzhorn, M.; Klyatskaya, S.; Ruben, M.; Wernsdorfer, W. *Nat. Nanotechnol.* **2013**, *8*, 165.

(6) Some reviews: (a) Rinehart, J. D.; Long, J. R. *Chem. Sci.* **2011**, *2*, 2078. (b) Sorace, L.; Benelli, C.; Gatteschi, D. *Chem. Soc. Rev.* **2012**, *42*, 3278. (c) Luzon, J.; Sessoli, R. *Dalton Trans.* **2012**, *41*, 13556.

(7) Some references for SMMs containing actinide ions: Rinehart, J. D.; Long, J. R. *J. Am. Chem. Soc.* **2009**, *131*, 12558. Rinehart, J. D.; Meihaus, K. R.; Long, J. R. *J. Am. Chem. Soc.* **2010**, *132*, 7572. Magnani, N.; Apostolidis, C.; Morgenstern, A.; Colineau, E.; Griveau, J.-C.; Bolvin, H.; Walter, O.; Caciuffo, R. *Angew. Chem., Int. Ed.* **2011**, *50*, 1696. Antunes, M. A.; Pereira, L. C. J.; Santos, I. C.; Mazzanti, M.; Marçalo, J.; Almeida, M. *Inorg. Chem.* **2011**, *50*, 9915.

(8) (a) Andruh, M.; Costes, J. P.; Diaz, C.; Gao, S. *Inorg.Chem.* **2009**, *48*, 3342 (Forum Article). (b) Sessoli, R.; Powell, A. K. *Coord. Chem. Rev.* **2009**, *253*, 2328. (c) Andruh, M. *Chem. Commun.* **2011**, *47*, 3015.

(9) Some reviews: (a) Guo, Y. N.; Xu, G. F.; Guo, Y.; Tang, J. *Dalton Trans.* **2011**, *40*, 9953. (b) Habib, F.; Mugeresu, M. *Chem. Soc. Rev.* **2012**, *42*, 3278. (c) Clemente-Juan, J. M.; Coronado, E.; Gaita-Ariño, A. *Chem. Soc. Rev.* **2012**, *41*, 7464.

(10) (a) Hewitt, I. J.; Tang, J.; Madhu, N. T.; Anson, C. E.; Lan, Y.; Luzon, J.; Etienne, M.; Sessoli, R.; Powell, A. K. *Angew. Chem., Int. Ed.* **2010**, *49*, 6352. (b) Blagg, R. J.; Muryn, C. A.; McInnes, E. J. L.; Tuna, F.; Winpenny, R. E. P. *Angew. Chem., Int. Ed.* **2011**, *50*, 6530. (c) Ishikawa, N.; Sugita, M.; Tanaka, N.; Ishikawa, T.; Koshihara, S. Y.; Kaizu, Y. *Inorg. Chem.* **2004**, *43*, 5498. (d) Takamatsu, S.; Ishikawa, T.; Koshihara, S. Y.; Ishikawa, N. *Inorg. Chem.* **2007**, *46*, 7250.

(11) (a) Rinehart, J. D.; Fang, M.; Evans, W. J.; Long, J. R. *Nat. Chem.* **2011**, *3*, 538. (b) Rinehart, J. D.; Fang, M.; Evans, W. J.; Long, J. R. *J. Am. Chem. Soc.* **2011**, *133*, 14236.

(12) Meihaus, K. R.; Rinehart, J. D.; Long, J. R. *Inorg. Chem.* **2011**, *50*, 8484.

(13) Ruiz, J.; Mota, A. J.; Rodríguez-Diéguez, A.; Titos, S.; Herrera, J. M.; Ruiz, E.; Cremades, E.; Costes, J. P.; Colacio, E. *Chem. Commum.* **2012**, *48*, 7916.

(14) (a) Colacio, E.; Ruiz, J.; Mota, A. J.; Palacios, M. A.; Cremades, E.; Ruiz, E.; White, F. J.; Brechin, E. K. *Inorg. Chem.* **2012**, *51*, 5857. (b) Colacio, E.; Ruiz, J.; Mota, A. J.; Palacios, M. A.; Ruiz, E.; Cremades, E.; Hänninen, M. M.; Sillanpää, R.; Brechin, E. K. *C. R. Chim.* **2012**, *15*, 878.

(15) Watanabe, A.; Yamashita, A.; Nakano, M.; Yamamura, T.; Kajiwara, T. *Chem.—Eur. J.* **2011**, *17*, 7428.

(16) Yamashita, A.; Watanabe, A.; Akine, S.; Nabeshima, T.; Nakano, M.; Yamamura, T.; Kajiwara, T. *Angew. Chem., Int. Ed.* **2011**, *50*, 4016.

(17) Altomare, A.; Burla, M.; Camalli, M.; Cascarano, G. L.; Giacovazzo, C.; Guagliardi, A.; Moliterni, A. G. G.; Polidori, G.; Spagna, R. *J. Appl. Crystallogr.* **1999**, *32*, 115.

(18) Sheldrick, G. M. *Acta Crystallogr., Sect. A* **2008**, *64*, 112.

(19) Farrugia, L. *J. Appl. Crystallogr.* **1999**, *32*, 837.

(20) *Topas-R, General profile and structure analysis software for powder diffraction data*; Bruker AXS: Göttingen, Germany.

(21) (a) Vallejo, J.; Cano, J.; Castro, I.; Julve, M.; Lloret, F.; Fabelo, O.; Cañadillas-Delgado, L.; Pardo, E. *Chem. Commun.* **2012**, *48*, 7726. (b) Langley, S. K.; Moubaraki, B.; Murray, K. S. *Inorg. Chem.* **2012**, *51*, 3947. (c) Sakamoto, S.; Fujinari, T.; Nishi, K.; Matsumoto, N.; Mochida, N.; Ishida, T.; Sunatsuki, Y.; Re, N. *Inorg. Chem.*, http:/dx.doi.org/101021/ic4008312l.

(22) Zhang, P.; Zhang, L.; Lin, S. Y.; Tang, J. *Inorg. Chem.*, http:/dx.doi.org/101021/ic400620j.

(23) Zhang, B.; Zheng, X.; Su, H.; Du, C.; Song, M. *Dalton Trans.* **2013**, *42*, 8571.

(24) Colacio, E.; Ruiz, J.; Lorusso, G.; Brechin, E. K.; Evangelisti, M. Manuscript in preparation

(25) Abragam, A.; Bleaney, B. *Electron Paramagnetic Resonance of Transition Ions*; Clarendon Press: Oxford, U.K., 1970.

(26) Shirivastava, K. N. *Phys. Status Solidi B* **1983**, *117*, 437.

(27) Wernsdorfer, W. *Supercond. Sci. Technol.* **2009**, *22*, 064013.

(28) Wernsdorfer, W.; Chakov, N. E.; Christou, G. *Phys. Rev. B* **2004**, *70*, 132413.

(29) Guo, Y. N.; Xu, G. F.; Wernsdorfer, W.; Ungur, L.; Gao, Y.; Tang, J.; Zhang, H. J.; Chibotaru, L. F.; Powell, A. K. *J. Am. Chem. Soc.* **2011**, *133*, 11948.